Materials Today Bio 32 (2025) 101731

Contents lists available at ScienceDirect

Materials Today Bio

journal homepage: www.journals.elsevier.com/materials-today-bio

pH/Hyal-responsive vancomycin-loaded chitooligosaccharide nanoparticles for intracellular MRSA infection treatment

Wenting Li [1], WeiWei Li [1], Xuanxiang Zhai, Xiao Liu, Xiaoyi Shi, Xiangjun Chen [*], Wei Hong [**]

School of Pharmacy, Shandong New Drug Loading & Release Technology and Preparation Engineering Laboratory, Binzhou Medical University, 346 Guanhai Road, Yantai, 264003, PR China

ARTICLE INFO

Keywords:
Antibiotics
Intracellular infection
Methicillin-resistant *S. aureus* (MRSA)
Macrophages
Targeted delivery

ABSTRACT

Staphylococcus aureus (*S. aureus*) is recognized as among the most critical bacterial pathogens globally. A significant portion of the complications associated with *S. aureus* infections arises from its ability to persist inside host phagocytes, particularly macrophages, making the eradication of intracellular *S. aureus* vital for therapeutic success. Regrettably, many antibiotics exhibit limited penetration into cells, underscoring the necessity for efficient intracellular delivery mechanisms. In this study, vancomycin-loaded chitooligosaccharide nanoparticles (COS@Van) coated with hyaluronic acid (HA), were engineered to function as an active-targeting antibiotic carrier recorded as HA/COS@Van. The HA coating serves as an external shell, which 1) covers the positive surface charge of COS NPs, thereby enhancing their biocompatibility and extending circulation time, and 2) facilitates targeted delivery to macrophages through specific interactions with the CD44 receptor. Confocal laser scanning microscopy (CLSM) and flow cytometry (FCM) experiments confirmed that HA/COS could effectively accumulate in methicillin-resistant *S. aureus* (MRSA) infected macrophages. Additionally, when administered intravenously in mouse models, HA/COS demonstrated markedly increased accumulation in the liver, the primary location of infected macrophages. These findings highlight the active-targeting capabilities of HA/COS both *in vitro* and *in vivo* settings. Consequently, after being loaded with Van, HA/COS@Van exhibited superior efficacy in killing intracellular MRSA *in vitro*, as compared to free Van. Furthermore, HA/COS@Van also demonstrated enhanced bactericidal activity in both mouse acute peritonitis model and mouse organ infection model. Therefore, this active-targeting delivery system may hold promise in advancing therapeutic outcomes for infections related to intracellular pathogens.

1. Introduction

The growing antimicrobial resistance presents a significant challenge to worldwide health systems. *Staphylococcus aureus* (*S. aureus*) remains a primary source of bacterial illnesses in community and hospital settings. Methicillin-resistant *S. aureus* (MRSA) represents a significant medical obstacle owing to its persistently elevated rates of illness and fatality [1–3]. While *S. aureus* has traditionally been regarded as an extracellular pathogen, mounting evidence suggests that it can survive intracellularly after being phagocytosed by macrophages, which may result in recurrence of infection and increased resistance [4,5]. *S. aureus* can support its survival by manipulating macrophage activation to M2 phenotype. Besides, M2 macrophages promote the formation of antibiotic-tolerant *S. aureus* small colony variant and lead to higher intracellular abundance. More concerning is the fact that bacteria surviving within host cells are shielded from the bactericidal effects of antibiotics. In reality, numerous antibiotics prove limited efficacy against intracellular pathogens owing to their minimal retention or poor intracellular accumulation [6–8]. Vancomycin, for example, which is often considered the treatment of last resort for MRSA, exhibits limited uptake by infected host cells. It is evident that, despite significant progress in antibiotic development, addressing intracellular bacterial infections remains a significant hurdle. Therefore, precise delivery of antimicrobial compounds to infected host cells, particularly macrophages, represents a vital approach for enhancing the efficacy of antibiotic therapies aimed at treating intracellular infections.

* Corresponding author.
** Corresponding author.
E-mail addresses: chenxj650@nenu.edu.cn (X. Chen), hongwei_sy@bzmc.edu.cn (W. Hong).
[1] These authors contributed equally to this work.

https://doi.org/10.1016/j.mtbio.2025.101731
Received 18 October 2024; Received in revised form 17 March 2025; Accepted 4 April 2025
Available online 8 April 2025

Nanotechnology offers promising opportunities to overcome the biopharmaceutical limitations of both small-molecule and biological drugs, markedly enhancing their efficacy [9–12]. Following this rationale, various nanodrug delivery systems have been explored to optimize the treatment of infectious diseases *via* systemic and localized routes of administration [13–16]. However, delivering antibiotics intracellularly to effectively eliminate bacterial pathogens still presents significant challenges. Chitooligosaccharide (COS), extracted from crustacean exoskeletons and fungal cell walls, stands as a prominent chitin derivative. This highly alkaline, naturally occurring, positively charged polysaccharide exhibits mucoadhesive characteristics [17,18]. The United States FDA has acknowledged COS as a biocompatible polymer appropriate for applications in tissue engineering and drug delivery systems. The application of COS-based nanoparticles (COS NPs) could potentially result in enhanced intracellular bacterial eradication due to several factors, including activation of immune system, active targeting of polarized macrophages, and their ability to escape lysosomal degradation [19–21]. However, the positive surface charge might impede the systemic use of COS NPs. Hyaluronic acid (HA), a non-toxic, biodegradable component of the extracellular matrix, is frequently employed as a targeting and capping agent. It specifically binds to CD44 receptor and can be broken down by hyaluronidase (Hyal) [22,23]. As known, numerous bacteria have been found capable of producing Hyal. Therefore, HA can function as a capping agent in reaction to the presence of Hyal within the bacterial infection microenvironment [24,25].

Herein, HA-capped vancomycin-loaded COS nanoparticles (HA/COS@Van) were developed as a nanocarrier for the treatment of intracellular bacterial infections. Investigations were carried out on cell compatibility, cellular uptake, intracellular trafficking, and cell polarization in RAW 264.7 cells. Additionally, the suppressive impact on MRSA growth, both *in vitro* and *in vivo*, was examined with regard to planktonic and intracellular infections, respectively. Both in a mouse peritoneal infection model and in a mouse organ infection model, infection was more effectively cured by HA/COS@Van than free Van, a common antibiotic in clinical treatment (Scheme 1).

2. Materials and methods

2.1. Materials

Comprehensive specifics concerning the materials employed in this investigation are provided in the Supplementary Material.

2.2. Methods

2.2.1. Preparation of HA/COS@Van

A total of 125 mg of COS was measured and solubilized in 10 mL of deionized (DI) water. Under ultrasonic conditions, 2.5 mL of PAA (10 mg/mL) was gradually introduced to the mixture to generate COS NPs. Subsequently, 1.5 mL of Van (5 mg/mL) was incorporated into the above

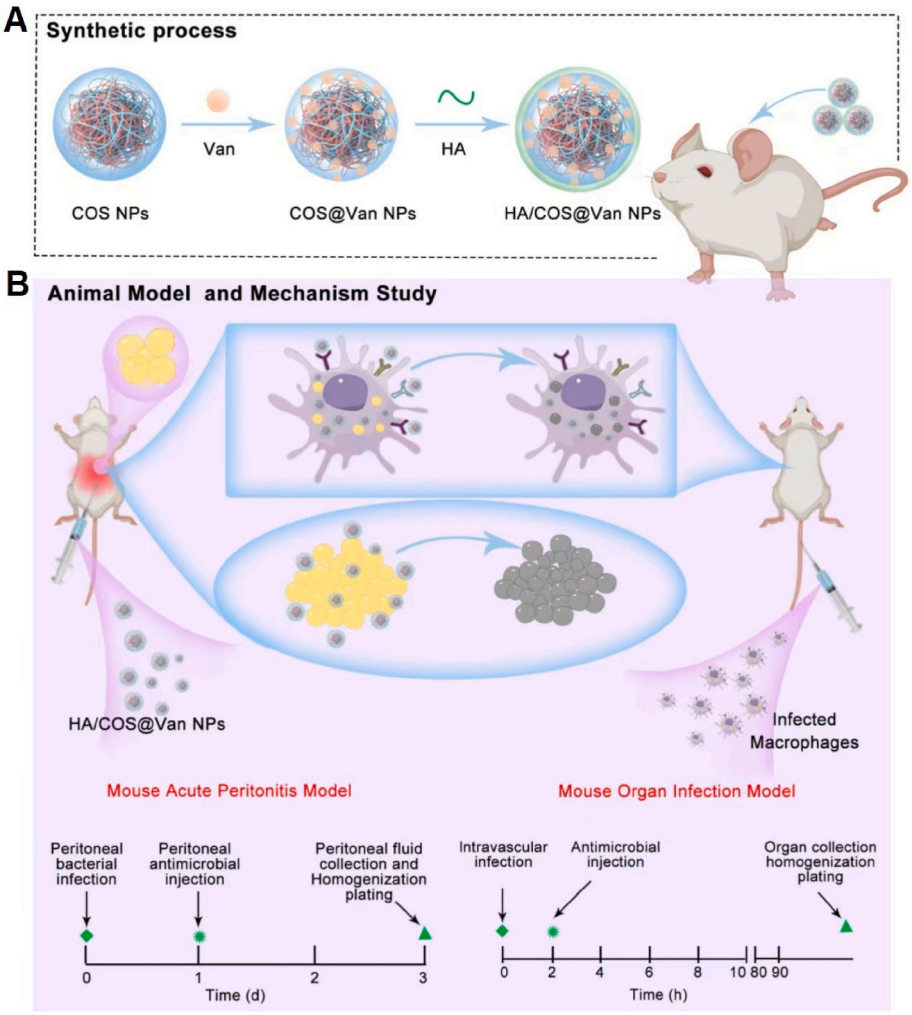

Scheme 1. Preparation of HA-capped vancomycin-loaded COS NPs (HA/COS@Van) (A). Eradication of intracellular MRSA by HA/COS@Van in a mouse acute peritonitis model and in a mouse organ infection model (B).

COS NPs solution, which underwent sonication for 5 min and continuous agitation for 6 h to yield COS@Van. Following this, HA/COS@Van was obtained by mixing COS@Van with HA or ^{FITC}HA at different weight ratios (5:1, 4:1, 3:1, 2:1, 1:1, 1:2 and 1:3), respectively. The mixture was vortexed for 3 min, continuously agitated for 2 h, then purified utilizing ultrafiltration at 4000 rpm for 20 min and re-dispersed in 10 mL of DI water.

2.2.2. Characterization of HA/COS@Van

The size and zeta potential of HA/COS@Van and absorbance of ^{FITC}HA/COS@Van with different weight ratios of COS@Van and HA or ^{FITC}HA were analyzed using the NanoBrook 90PlusPALS analyzer (USA) or TU-1810 ultraviolet–visible spectrophotometer (Purkinje, China), respectively. The morphological characteristics of COS NPs, COS@Van and HA/COS@Van were observed with the JEOL JEM1400 TEM (Japan). The structure and interaction of HA/COS were analyzed using a Fourier transform infrared (FTIR) spectrometer (Nicolet IS10, Co., America). The encapsulation efficiency (EE%) of Van was computed using Equation (1). The absorbance at 282 nm was ascertained to quantify the concentration of Van.

$$DL\% = \frac{\text{Weight of Van in NPs}}{\text{Weight of feeding Van}} \times 100\% \quad (1)$$

The prepared COS@Van and HA/COS@Van were utilized to investigate Van's release profile within the nanocomposite by employing dialysis. Specifically, the prepared HA/COS@Van and COS@Van were enclosed in a dialysis bag (MW = 1000), and 0.1 mol/L phosphate-buffered solution (pH 7.4, 5.5 and 5.5+Hyal) was used as the release medium, respectively. At predefined intervals, 3 mL of dialysis solution was extracted, and an equivalent volume of fresh PBS was replenished. The cumulative release of Van was assessed using UV spectroscopy, with the results presented as mean ± SD.

2.2.3. Targeted binding of NPs toward planktonic MRSA

The bacterial adhesion of NPs was evaluated by incubating MRSA suspensions with fluorescent NP@RHB (COS@RHB and HA/COS@RHB), which had been infused with Rhodamine B (RHB) as a fluorescent probe. Free RHB was utilized as a control. After incubation for 0.5 h, the fluorescence of RHB was examined utilizing an Olympus BX53F2 Fluorescent Microscope (Japan) and a BD FACSCanto II flow cytometer (USA), respectively.

2.2.4. Evaluation of antibacterial activity

2.2.4.1. Minimum inhibitory concentration (MIC) and minimum bactericidal concentration (MBC). The MICs of various formulations, encompassing free Van, COS@Van, HA/COS@Van and HA/COS@Van + Hyal, were determined using the micro-dilution method against MRSA (1×10^5 CFU/mL) at pH levels of 5.5 and 7.4, ranging in concentrations from 0.25 to 64 μg/mL. Bacterial suspensions were utilized as a negative control to establish a baseline. The measurements were conducted utilizing six separate repetitions to guarantee accuracy.

The minimum bactericidal concentrations (MBC) of free Van, COS@Van, HA/COS@Van and HA/COS@Van + Hyal were also determined at pH 7.4 and 5.5, respectively. The concentration of Van ranged from 0.25 to 64 μg/mL. Viable bacteria were determined after 24 h incubation at 37 °C. The MBC was defined as the lowest concentration that killed 99.9 % of original inoculum.

2.2.4.2. Live/dead assay. Bacterial viability was assessed utilizing a BacLight Bacterial Viability Kit on samples treated at pH 5.5. These samples included free Van, COS@Van, HA/COS@Van, and HA/COS@Van + Hyal at pH 5.5. The Van concentration was maintained at 2 μg/mL, followed by overnight incubation. After incubation, bacterial samples underwent staining with a dye blend comprising propidium iodide and SYTO 9 in a 1:1 ratio. The staining was executed for 30 min at a steady temperature of 25 °C. Fluorescent micrographs were procured utilizing an Olympus BX53F2 Fluorescent Microscope (Japan).

2.2.4.3. Observation with scanning electron microscopy (SEM). The impact of various formulations on bacterial suspensions was additionally examined using SEM. MRSA was cultivated at 37 °C for 12 h under different treatments, including free Van, COS@Van, HA/COS@Van, and HA/COS@Van + Hyal at pH 5.5. The formulations containing Van were set at a concentration of 2 μg/mL, succeeded by overnight treatment with 2.5 % glutaraldehyde. After incubation, the bacterial samples were mixed, gradually dehydrated, coated with gold, and analyzed utilizing a Zeiss EVO LS15 SEM (Germany).

2.2.5. Cellular uptake

For flow cytometry (FCM) analysis, RAW264.7 cells were grown in 6-well plates at 1×10^6 cells per well and exposed to RHB-loaded NPs, including COS@RHB, HA/COS@RHB + Hyal (0.5 h), HA/COS@RHB + Hyal (4 h) and free RHB for 0.5 h, respectively. After exposure, the cells were harvested, rinsed thrice with PBS, resuspended in 1 mL of PBS, and analyzed by FCM. For microscopic examination, RAW264.7 cells (1×10^6 cells/well) were placed on coverslips in 6-well plates and left overnight. The treatment of cells followed the procedure outlined for FCM. Upon completion of the uptake process, the cells underwent three rinses with PBS, after which the nuclei were labeled utilizing Hoechst 33258 for 15 mi and observed by an Olympus BX53F2 Fluorescent Microscope (Japan).

2.2.6. Intracellular antibacterial activity study

RAW264.7 cells were placed in 24-well plates at 3×10^5 cells per well and left overnight in a 37 °C, 5 % CO_2 environment. MRSA was subsequently introduced into the cell culture medium of RAW264.7 cell culture medium at a 20:1 bacteria-to-cell ratio and kept for 4 h at 37 °C. To eliminate extracellular bacteria, gentamicin (50 μg/mL) was introduced. The infected cells were then treated with saline, free Van, COS@Van, HA/COS@Van, and HA/COS@Van + Hyal with the Van concentration of 4 μg/mL. Following 12 h of exposure, the medium was removed, and cells were promptly rinsed twice with PBS. Afterwards, cells underwent lysis with 0.5 % Triton X-100 for 15 min, which was succeeded by centrifugation to extract the supernatant. The count of viable intracellular bacteria was ascertained by culturing on tryptic soy agar plates.

2.2.7. Antibacterial mechanism of HA/COS@Van

2.2.7.1. Nanoparticle co-localization in infected RAW264.7 cells. RAW 264.7 cells underwent infection with ^{sfGFP}MRSA for 4 h in 6-well chamber slides. Following infection, gentamicin (50 μg/mL) was added for a 1.5 h incubation to eliminate extracellular bacteria. The cells were then exposed to RHB-labeled NPs for 0.5 h. Following this, the cells underwent staining with Hoechst 33258 for 15 min. Afterwards, the cells were rinsed twice using a PBS solution. Ultimately, the cells were observed using a Zeiss LSM 880 laser confocal microscope (CLSM).

2.2.7.2. Lysosomal escape. Lysosomal escape behavior was investigated in RAW264.7 cells. Cells (1×10^6/well) were placed in 6-well plates and kept at 37 °C for 24 h. COS@RHB or HA/COS@RHB was then added, and it was succeeded by incubation at 37 °C for 0.5 h and 4 h, respectively. LysoTracker green staining was applied for 40 min, and the cells were rinsed 2–3 times with PBS. Ultimately, the cells were exposed to Hoechst 33258 for 15 min and subsequently rinsed twice with PBS. The observations were conducted utilizing a Zeiss LSM 880 laser confocal microscope (CLSM).

2.2.7.3. Membrane potential (MP) detection. The bacterial MP was

assessed utilizing the BacLight bacterial MP kit. Plasma MP of MRSA was examined following treatment with CCCP, COS NPs, and HA/COS in the presence or absence of Hyal, respectively. The COS concentration was kept at 50 μg/mL. After incubation, 3,3′-diethyloxacarbocyanine ($DiOC_2(3)$) was added to the suspensions, followed by an additional incubation of 30 min. Changes in red/green fluorescence intensity were carefully measured using a BD FACSCanto II flow cytometer (USA).

2.2.7.4. Outer membrane permeabilization assay. The N-Phenyl-1-naphthylamine (NPN) uptake assay was utilized to assess outer membrane permeability. NPN was introduced to MRSA bacterial suspensions to attain a final concentration of 10 μM. Initial fluorescence levels were recorded using a Tecan Infinite M200 PRO multifunctional microplate reader, operating at specific excitation and emission wavelengths (350 nm and 420 nm). The bacterial suspensions were subsequently exposed to COS NPs and HA/COS, with and without Hyal, at the concentrations outlined in Section 2.2.7.3. The fluorescence enhancement following treatment was determined utilizing the forementioned method.

2.2.7.5. Pro-inflammatory immunomodulatory. RAW264.7 cells (1×10^6 per well) were placed into 6-well plates, and the medium was substituted with a new medium comprising saline, free Van, COS NPs, COS@Van, or HA/COS@Van. After co-incubation at 37 °C for 24 h, the cells were incubated with CD86 for 20 min. Following PBS washing, Hoechst 33258 staining was applied for 15 min, and the cells were observed utilizing CLSM. The same culture method described above was also employed to measure the secretion levels of antibodies against tumor necrosis factor (TNF)-α and interleukin (IL)-6 using ELISA kits.

2.2.8. In vitro and in vivo biocompatibility

2.2.8.1. In vitro cytotoxicity and hemolysis assay. The cytotoxicity of HA/COS@Van and COS@Van was evaluated in RAW 264.7 cells using the 3-(4,5-dimethyl-2-thiazolyl)-2,5-diphenyl-2-H-tetrazolium bromide (MTT) assay. RAW 264.7 cells were placed into 96-well plates and incubated at 37 °C for 24 h. The medium was then substituted with a fresh medium comprising different concentrations of HA/COS@Van and COS@Van (4–256 μg/mL), respectively. Following a further 24-h incubation at 37 °C, 10 μL of MTT (5 mg/mL) was introduced, and the cells were cocultured for 4 h. Following this, the DMSO solution was introduced and placed on a shaker at 37 °C for 10 min. These crystals' absorbance was subsequently quantified at 490 nm employing a BioTek Synergy H1 hybrid multimode microplate reader (USA). The average percentage of CV was computed, with all data denoted as the mean ± SD.

To assess the hemolytic potential of HA/COS@Van and COS@Van, the method described in our earlier study [26]. The hemolysis percentage was determined utilizing Equation (2):

$$\text{Hemolysis}\ (\%) = \frac{OD_t - OD_0}{OD_{100} - OD_0} \times 100\% \quad (2)$$

Where OD_t represents the absorbance of rRBCs exposed to HA/COS@Van or COS@Van at concentration t, OD_0 refers to the absorbance of rRBCs exposed to saline, and OD_{100} indicates the absorbance of rRBCs exposed to 0.5 % Triton X-100.

2.2.8.2. In vivo acute toxicity. Male BALB/c mice were injected intravenously with HA/COS@Van once a day for 3 days, while the control group received saline injections. The Van dose in HA/COS@Van group was equivalent to 25 mg/kg which exceeds the *in vivo* experimental dose utilized in this investigation five times. On the 4th day post-injection, all mice were euthanized. Major organs, including the heart, lungs, kidneys, liver, and spleen, were collected for H&E staining and then examined under an optical microscope to evaluate potential *in vivo* toxicity.

2.2.9. In vivo biodistribution and antibacterial effect in MRSA-infected mice

2.2.9.1. In vivo targeting study. RHB-labeled HA/COS were administered *via* tail vein injection into BALB/c mice to investigate the biodistribution of HA/COS. The *ex vivo* fluorescence images of organs were subsequently observed at diverse time points (0.5 h, 1 h, 3 h and 24 h) utilizing an IVIS® Spectrum imaging system (PerkinElmer, USA).

2.2.9.2. In vivo therapeutic effect. The *in vivo* antimicrobial effectiveness of HA/COS@Van was firstly examined utilizing an MRSA-infected acute peritonitis model in mice. Mice were initially injected intraperitoneally (*i.p.*) with MRSA (5×10^7 CFU/mouse, 100 μL). Following 24 h of infection, the mice were arbitrarily separated into four groups (6 mice/group): (i) saline, (ii) free Van, (iii) COS/Van, and (iv) HA@COS/Van. Every group was administered a single intraperitoneal injection of the designated treatment, standardized to 200 μL per formulation. The Van doses in the NP groups were equivalent to 5 mg/kg. Post-treatment, all mice were euthanized, peritoneal macrophages were collected by washing the peritoneal cavity with 5 mL cold PBS. Macrophages cells were collected by centrifugation at 4 °C, 1300 rpm for 10 min, and the collected cell precipitate was re-dispersed with pre-cooled saline and centrifuged at 900 rpm for 3 min to collect the cells again. Finally, macrophages were lysed by homogenization. The number of surviving peritoneal bacteria was determined by plating on tryptic soy agar plates.

Mouse organ infection model was also established to evaluate the killing of MRSA by HA@COS/Van. The peritoneal infection model was established to isolate peritoneal macrophages containing *in vivo* internalized MRSA. For this, MRSA was administered to eight-week-old male BALB/c mice. To acquire macrophages containing internalized MRSA, peritoneal fluid was extracted 24 h following MRSA inoculation, yielding 5×10^7 macrophages/mL. These MRSA-laden macrophages were subsequently introduced into mice *via* intravenous injection to establish mouse organ infection model. Then, a single administration of saline, free Van, COS/Van, or HA@COS/Van was administered to the mice 2 h post-infection. The Van doses in the NP groups were equivalent to 5 mg/kg. On the 4th day post-treatment, the mice were collected, and diverse organs were harvested, homogenized, and plated.

2.2.10. Statistical analyses

Data were denoted as the mean ± standard deviation (S.D.). Differences between the two groups were analyzed utilizing the Student's t-test. Statistical significance was denoted as follows: $^*p < 0.05$, $^{**}p < 0.01$, $^{***}p < 0.001$, and $^{****}p < 0.0001$.

3. Results and discussions

3.1. Preparation and characterization of HA/COS@Van

First, positively charged chitooligosaccharide (COS) and negatively charged polyacrylic acid (PAA) were employed to fabricate COS NPs, given that COS and PAA can spontaneously form nanoparticles in aqueous media through electrostatic interactions. As illustrated in Fig. 1A, the morphology of the resultant COS NPs revealed a spherical morphology with an approximate average diameter of 155 nm. The zeta potential of these COS NPs was measured at +25 mV, which was attributed to the abundance of secondary and primary amine groups present in the chitooligosaccharide chains. The incorporation of Van did not alter the particle size and zeta potential of COS@Van, maintaining a diameter of roughly 160 nm and a zeta potential of +22 mV (Fig. 1B). HA/COS@Van with varying weight ratios of HA and COS@Van were subsequently produced in order to fine-tune both particle size and surface charge. As depicted in Fig. 1C, it was evident that the zeta potential consistently decreased while particle size increased until the HA loading content reached a ratio of 1:1. Beyond this ratio, further increases in HA

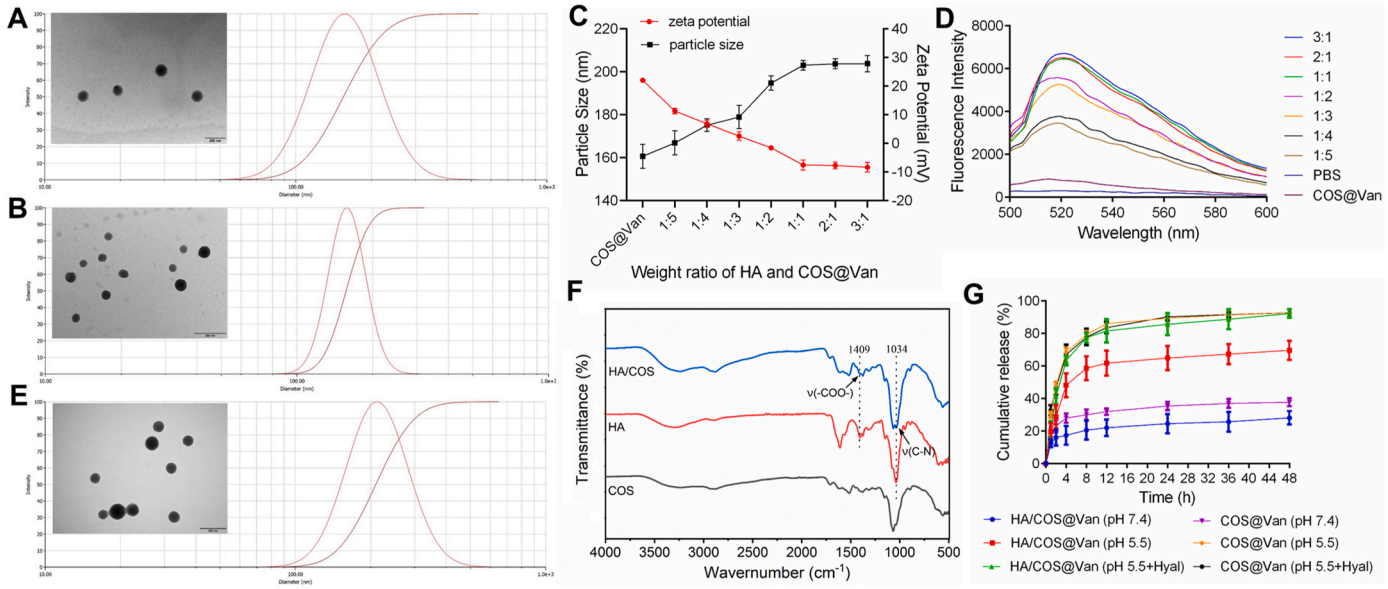

Fig. 1. The particle sizes and TEM images of COS NPs (A) and COS@Van (B). The particle size and zeta potential of HA/COS@Van with different weight ratios of HA and COS@Van (C). The fluorescence intensity of ^{FITC}HA/COS@Van with different weight ratios of ^{FITC}HA and COS@Van (D). The particle size and TEM image of HA/COS@Van with the weight ratio of 1:1 (E). FTIR spectra of HA, COS NPs and HA/COS (F). The cumulative drug release behavior of Van from HA/COS@Van and COS@Van under different conditions (G).

content caused the surface charge and particle size to plateau, potentially attributed to the saturation of electrostatic adsorption of HA. Additionally, FITC labeled HA was also selected to determine the capping of HA on COS NPs. As shown in Fig. 1D, the fluorescence intensity was proportional to the HA loading content until the weight ratio reached 1:1, consistent with particle size and zeta potential results. Consequently, HA/COS@Van (1:1), with a particle size of approximately 200 nm and a zeta potential of −8.5 mV, was selected for further investigation. The prepared HA/COS@Van exhibited a spherical shape, with particles demonstrating a uniform size distribution (Fig. 1E). Additionally, the characteristic peaks at 1409 cm^{-1} (ν-COO-) and 1034 cm^{-1} (νC-N), corresponding to hyaluronic acid, were present in the HA/COS FTIR spectrum (Fig. 1F). Moreover, the encapsulation efficiency of Van within the HA/COS@Van was 67.07 %.

Considering the pH sensitivity and Hyal-specific degradation of COS NPs and HA shell, it is anticipated that HA/COS@Van would disintegrate under acidic and enzymatic conditions, such as those found in infection microenvironments, thereby triggering the collapse of both the inner core and outer shell. Thus, it was hypothesized that the pH/Hyal-sensitive breakdown of HA/COS would result in a pH/Hyal-responsive release of Van. Consistent with expectations, the cumulative release of Van from HA/COS@Van at pH 7.4 was found to be approximately 30 %. In contrast, nearly 70 % of Van was released rapidly at lower pH values, while the cumulative release of Van exceeded 90 % in the presence of Hyal (Fig. 1G). Moreover, it could be noted that the release behavior of Van from COS@Van was accelerated at pH 7.4 and 5.5 compared with that of HA/COS@Van, suggesting the stabilizing capability of HA shell. However, there was no difference in the releasing behavior between HA/COS@Van and COS@Van under acidic and enzymatic condition (pH 5.5+Hyal), which might be due to the collapse of the HA shell. Taken together, these findings demonstrated that HA/COS@Van could maintain stability under physiological pH conditions and underwent rapid degradation in response to acidic and enzymatic environments, facilitating Van release and leading to targeted effects while minimizing off-target toxicity in normal tissues.

3.2. Bacterial binding affinity and extracellular antibacterial activity

The bacterial targeting capacity of the formulated RHB-loaded NPs was examined using fluorescent microscopy (FM). The NP@RHB/bacteria suspension was incubated in a shaker at 37 °C for 0.5 h to facilitate the binding of NP@RHB to bacteria. As depicted in Fig. 2A, the RHB-loaded NP-treated groups displayed more intense fluorescence after coincubation compared to free RHB. Among the tested agents, COS/RHB exhibited the highest fluorescence intensity due to its positive surface charge. HA/COS@RHB demonstrated increased fluorescence intensity in the presence of Hyal, which was attributed to the degradation of the HA shell, resulting in an enhanced surface charge. Furthermore, a comparison of bacteria-associated fluorescence between 0.5 h and 4 h after exposure in the presence of Hyal revealed similar fluorescence intensities at both time points, a little weaker than that of COS@RHB. Flow cytometry (FCM, Fig. 2B) was employed to quantitatively confirm the binding of the prepared NPs to bacteria. Consistent with the FM results, FCM analysis showed that the COS@RHB group exhibited the highest fluorescence intensity, followed by HA/COS@RHB + Hyal, HA/COS@RHB, and free RHB. Additionally, rapid saturation of fluorescence was observed, with approximately 85 % of maximal binding achieved within 0.5 h in the presence of Hyal. This suggests that even a brief exposure at the infection site may suffice for bacterial binding when utilizing HA/COS.

Next, the antibacterial effects of free Van, COS@Van, HA/COS@Van, and HA/COS@Van + Hyal against planktonic MRSA were investigated. The results (Table 1) indicated that free Van exhibited the strongest antibacterial activity with a MIC of 1 μg/mL at pH 7.4. The MICs of COS@Van, HA/COS@Van, and HA/COS@Van + Hyal were determined to be 4, 8, and 4 μg/mL, respectively. Van-loaded NPs required higher initial Van concentrations compared to the free drug to achieve comparable antibacterial effects at physiological pH, which may be attributed to the sustained drug release characteristics. As expected, all Van-loaded NPs showed markedly enhanced activity at pH 5.5. HA/COS@Van + Hyal demonstrated comparable antibacterial potency as that of free Van, indicating that the accelerated release under acidic and enzymatic conditions could improve its antibacterial efficacy. For MBC assay, similar results were obtained, except for the MBC values of COS@Van and HA/COS@Van + Hyal at pH 5.5. Both COS@Van and HA/COS@Van + Hyal showed even stronger bactericidal capability than that of free Van, with the MBC value of 2 μg/mL, which might be due to the enhanced NP-bacterium electrostatic interactions. These

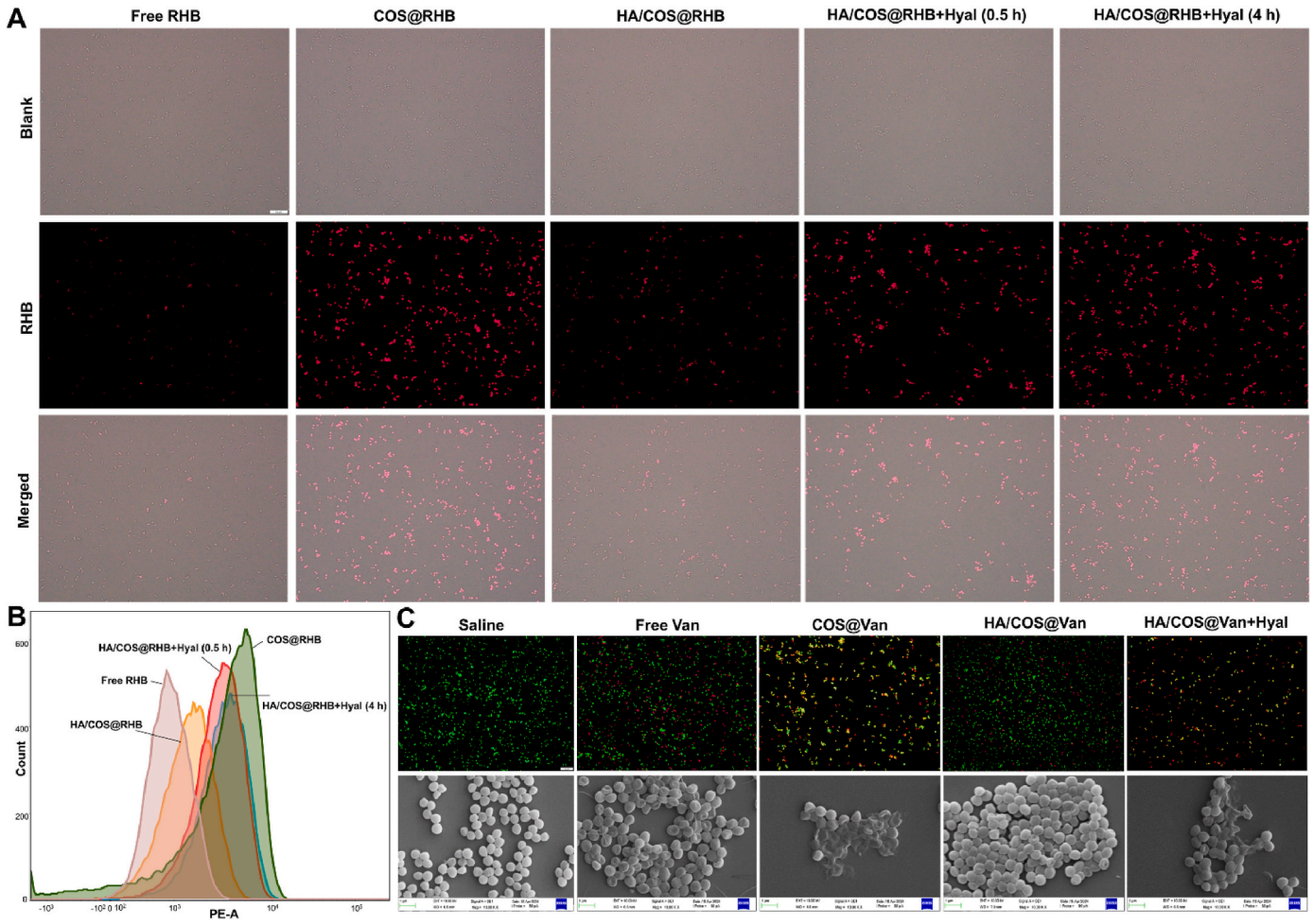

Fig. 2. Bacterial binding affinity between planktonic MRSA and free RHB, COS@RHB, HA/COS@RHB, HA/COS@RHB + Hyal (0.5 h) and HA/COS@RHB + Hyal (4.0 h) as observed *via* fluorescence microscope (A) and flow cytometry (B). Live/Dead fluorescence images and SEM images of MRSA following overnight exposure to saline, free Van, COS@Van, HA/COS@Van and HA/COS@Van + Hyal (C). Scale bar = 50 μm.

Table 1
Antibacterial effects of tested agents against MRSA.

Tested Agents	MIC (μg/mL)		MBC (μg/mL)	
	pH 7.4	pH 5.5	pH 7.4	pH 5.5
free Van	1	1	4	4
COS NPs	>1600	>1600	>1600	>1600
COS@Van	4	1	16	2
HA/COS@Van	8	2	32	8
HA/COS@Van + Hyal	4	1	16	2

interactions, as demonstrated, might facilitate the entry of released Van through the compromised bacterial cell membrane. Moreover, considering the lower toxicity of HA/COS@Van, further underscored the potential of this delivery system for treating infections. Although several studies have confirmed the antibacterial potential of COS NPs [27–29], the COS NPs alone exhibited limited killing effects, possibly due to the low concentrations used in this study (<1600 μg/mL).

A Live/Dead assay was subsequently utilized to observe cell viability following exposure to the evaluated compounds at a 2 μg/mL dose under a pH of 5.5, simulating the bacterial microenvironment. Upon exposure to HA/COS@Van in the presence of Hyal, MRSA cells were effectively eradicated, as confirmed by the appearance of merged yellow cellular fluorescence (Fig. 2C). To further assess bacterial morphological changes after various treatments, SEM imaging was employed. In the blank control group (saline), MRSA organisms retained their typical morphology and unblemished exteriors. Conversely, exposure to HA/COS@Van combined with Hyal resulted in notable alterations to bacterial form and textured surfaces, along with enhanced efflux of cellular components, suggesting its robust capacity for eliminating planktonic MRSA.

3.3. Cellular uptake and intracellular antibacterial activity

MRSA can invade mammalian cells, survive within them, and replicate after ingestion, making the treatment of such infections more challenging. The intracellular distribution of HA/COS@RHB in RAW264.7 cells was assessed using both FM and FCM. As depicted in Fig. 3A, markedly stronger fluorescence intensities were observed in all RHB-loaded NPs compared to free RHB. This may be attributed to the mannose receptor and CD44 receptor on the cell surface, which likely facilitates the uptake into macrophages. A similar trend was seen in the FCM assay, where the fluorescence intensities of all RHB-loaded NPs substantially exceeded those of free RHB (Fig. 3B).

As the formulated NPs were capable of enhancing drug delivery into macrophages, their efficacy in eradicating intracellular MRSA within RAW 264.7 cells infected for 4 h was assessed by enumerating the CFU of persisting intracellular bacteria. Following a 24-h treatment, all Van-encapsulated NPs exhibited markedly more potent suppressive effects against intracellular bacteria in comparison to unencapsulated Van in MRSA-infected macrophages (Fig. 3C). Free Van exhibited limited inhibitory activity, presenting the highest CFU among the tested agents,

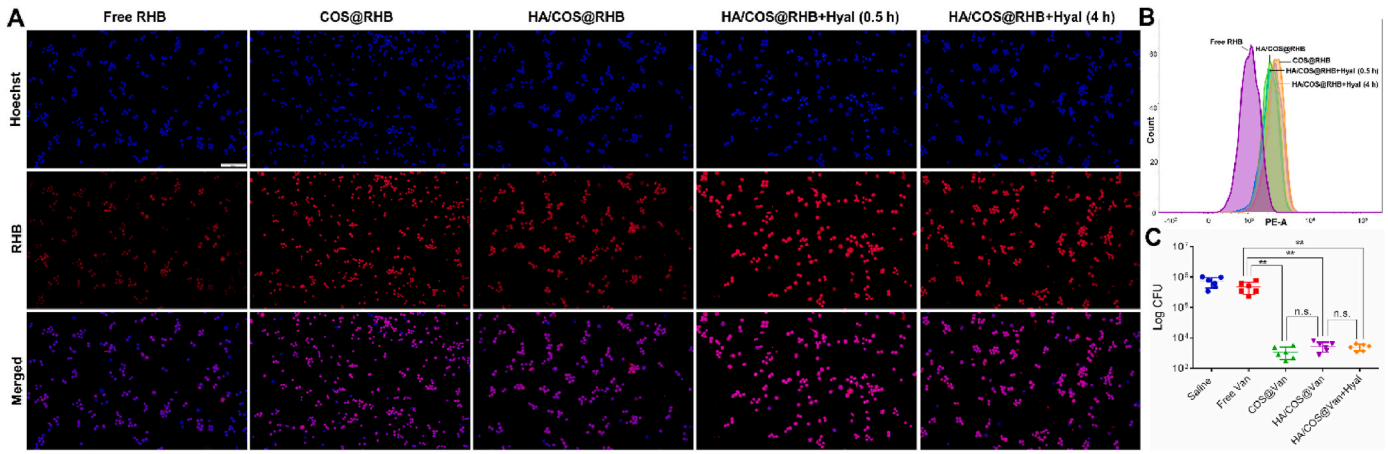

Fig. 3. Cellular uptake of HA/COS@RHB by RAW 264.7 cells. The photos were taken with fluorescence microscopy (A), and the mean fluorescence intensity of cells was ascertained by flow cytometric analyses (B) after incubation with free RHB, COS/RHB, HA/COS@RHB, HA/COS@RHB (0.5 h) and HA/COS@RHB (4 h) at the same dose of RHB. Effects of free Van, COS@Van, HA/COS@Van, and HA/COS@Van + Hyal on intracellular MRSA in infected RAW 264.7 cells (C). Scale bar = 50 μm.

except for the untreated control group. These findings indicated that efficient delivery of Van to MRSA-infected RAW 264.7 cells could significantly kill intracellular bacteria.

3.4. The antibacterial mechanism of HA/COS@Van

3.4.1. Nanoparticle co-localization and intracellular trafficking in infected RAW264.7 cells

It is well-documented that MRSA can enter a quiescent phase after invading host cells, allowing it to survive intracellularly and often contributing to treatment failure. To explore this, RAW 264.7 macrophages infected with ^{sfGFP}MRSA were employed as model phagocytes to examine the capacity of HA/COS to actively target intracellular MRSA. As shown in Fig. 4A, cells infected with ^{sfGFP}MRSA and treated with HA/COS@RHB exhibited markedly stronger red fluorescence relative to those exposed to free RHB. Additionally, the distinct co-localization of green and red fluorescence signals suggested that HA/COS@RHB not only effectively crossed the cell membrane barrier but also localized to intracellular MRSA.

Chitooligosaccharide (COS), a polycation, has been reported to enable endosomal/lysosomal escape due to the "proton-sponge" effect, attributed to its relatively high pK_a value of 6.0–6.5 resulting from primary amine groups present in its side chain. To obtain a more comprehensive insight into the intracellular trafficking pathways of HA/COS, we examined the co-localization of fluorescent NP signals with acidic compartments, such as lysosomes, which were tracked using LysoTracker green (Fig. 4B). It was observed that both COS NPs and HA/COS exhibited strong green fluorescence signals after 0.5 h of incubation, indicating receptor-mediated endocytosis. As the incubation period extended to 4 h, the intensity of green fluorescence weakened in both COS NPs and HA/COS treated groups, suggesting that lysosomal escape occurred following initial entry into lysosomes. Moreover, the HA shell did not impede the lysosomal escape behavior of HA/COS, which might be due to the enzymatic degradation of HA in lysosome.

3.4.2. Membrane susceptibility assay

Prior research has demonstrated that antibacterial agents with positive charges can disrupt cellular membranes. Investigations using electron microscopy on diverse bacterial species have revealed the interplay between COS and bacterial cell surfaces [19,30,31]. Consequently, the interaction of positively charged primary amine group (NH_3^+) of COS with bacterial cell membranes carrying negative charges results in enhanced membrane permeability, causing the release of intracellular components and eventually leading to cellular demise. As mentioned earlier, while COS NPs alone did not exhibit bactericidal activity, the enhanced activity of COS@Van may be attributed to the improved NP-bacterium interactions, which compromise the bacterial membrane and allow more Van to translocate through the membrane. To assess membrane potential (MP) changes in MRSA, the BacLight bacterial membrane potential kit was employed. As noted in the introduction, $DiOC_2(3)$ was used to analyze the inner membrane potential. This dye emits red fluorescence when self-associated in an intact membrane and green fluorescence when it exists in a monomeric state in a depolarized membrane. As shown in Fig. 4C, COS NPs exhibited a notable rise in green fluorescence intensity, both with and without Hyal, indicating depolarization of the inner bacterial membrane. The HA/COS group displayed moderate MP alterations without Hyal, while comparable MP changes to COS NPs were observed in the HA/COS group in the presence of Hyal. Additionally, outer membrane permeability was evaluated utilizing NPN as a fluorescence probe. Fig. 4D shows a marked increase in NPN fluorescence intensity following incubation with COS NPs, both in the presence and absence of Hyal. However, HA/COS also increased outer membrane permeability, but only in the presence of Hyal, suggesting that membrane alterations were induced. These results indicated that in the presence of Hyal, HA/COS@Van can effectively achieve MRSA eradication through a combination of chemotherapy, MP alteration, and induced outer membrane permeabilization.

3.4.3. Pro-inflammatory immunomodulatory

Macrophages, a vital class of immune cells, serve a pivotal function in resolving inflammation and regenerating tissue. In mammals, these cells can differentiate into either pro-inflammatory M1 or anti-inflammatory M2 phenotypes, contingent on environmental signals. With the deeper understanding of intracellular infectious diseases, a relationship between anti-inflammatory M2 macrophage phenotypes and persistent intracellular infections has been gradually identified. Given the important role of M2 macrophages in persistent MRSA infections, Given the important role of M2 macrophages in persistent MRSA infection, immunomodulation basing on macrophage repolarization may be a promising strategy for intracellular MRSA therapy. COS has been demonstrated to trigger the secretion of pro-inflammatory mediators in macrophages, thus initiating an appropriate immune reaction against intracellular pathogens. The pro-inflammatory immunomodulatory impact of COS NPs was further examined using immunofluorescence techniques. M1 macrophages, identified by CD86 expression, actively participate in microbicidal functions and generate pro-inflammatory mediators such as interleukin-6 (IL-6), TNF-α, and interleukin-12 (IL-12). As illustrated in Fig. 4E, compared to the control

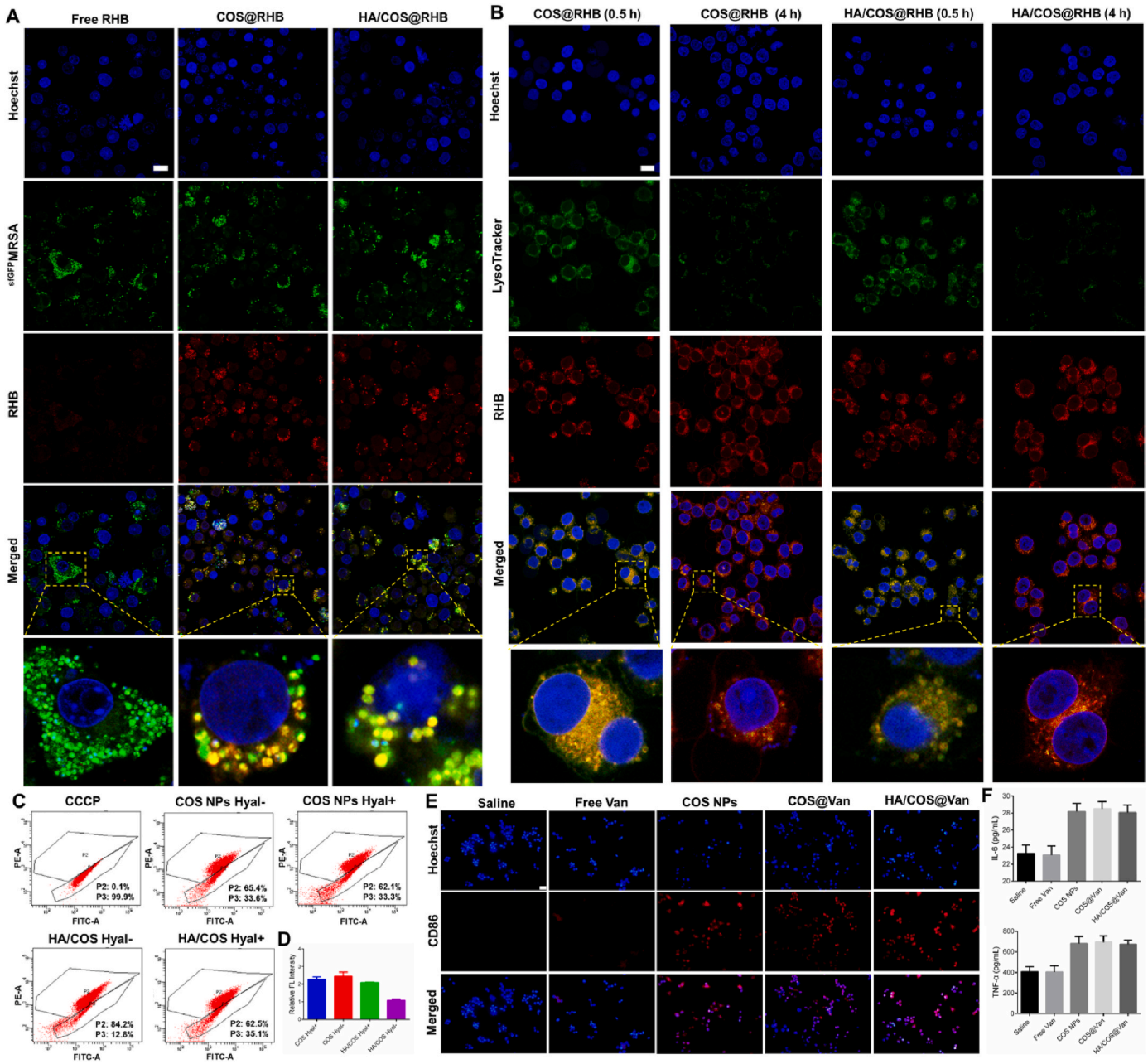

Fig. 4. Intracellular targeting ability of free RHB, COS@RHB, and HA/COS@RHB. Scale bar = 20 μm (A). Co-localization observation of the COS@RHB and HA/COS@RHB with LysoTracker in RAW 264.7 cells after 0.5 h- and 4 h-incubation by CLSM. Scale bar = 20 μm (B). Evaluation of cytoplasmic membrane potential (C) and outer membrane permeability (D) after treatment with COS NPs and HA/COS in the presence and absence of Hyal. Immunofluorescent staining of RAW 264.7 cells post-incubation with saline, free Van, COS NPs, COS@Van, or HA/COS@Van (E). Quantitative analysis of IL-6 and TNF-α levels utilizing enzyme-linked immunosorbent assay (F).

group, increased CD86 expression (red fluorescence) was noted in the groups treated with COS NPs, COS@Van, and HA/COS@Van, suggesting that COS induces macrophage polarization toward the M1 phenotype. Similarly, RAW264.7 cells cultured with COS NPs, COS@Van, and HA/COS@Van secreted higher levels of IL-6 and TNF-α, confirming that COS possesses pro-inflammatory immunomodulatory properties. These findings demonstrate that COS can polarize macrophages toward the M1 phenotype, thereby enhancing antibacterial immunity.

3.5. *In vitro and in vivo toxicity*

The biocompatibility of HA/COS@Van was evaluated in both *in vitro* and *in vivo* models. For *in vitro* assessment, biocompatibility was examined *via* cell viability and hemolysis assays (Fig. 5A). Cytotoxicity toward RAW264.7 cells was ascertained utilizing the MTT assay, where HA/COS@Van displayed minimal toxicity. At a 256 μg/mL concentration, over 85 % of RAW264.7 cells remained alive, a percentage markedly exceeding that required at clinical doses. Additionally, the hemolytic potential of HA/COS@Van was assessed, and no substantial hemolytic effects were observed, even at the highest tested level, suggesting strong blood compatibility (Fig. 5B). These results suggest that HA/COS@Van is well-suited for systemic administration. In contrast, COS@Van exhibited mild hemolytic activity at a 256 μg/mL concentration (>15 %), which may be attributed to its positive surface charge.

To evaluate the *in vivo* toxicity of HA/COS@Van, major organs (heart, liver, spleen, lung, and kidney) from BALB/c mice were procured

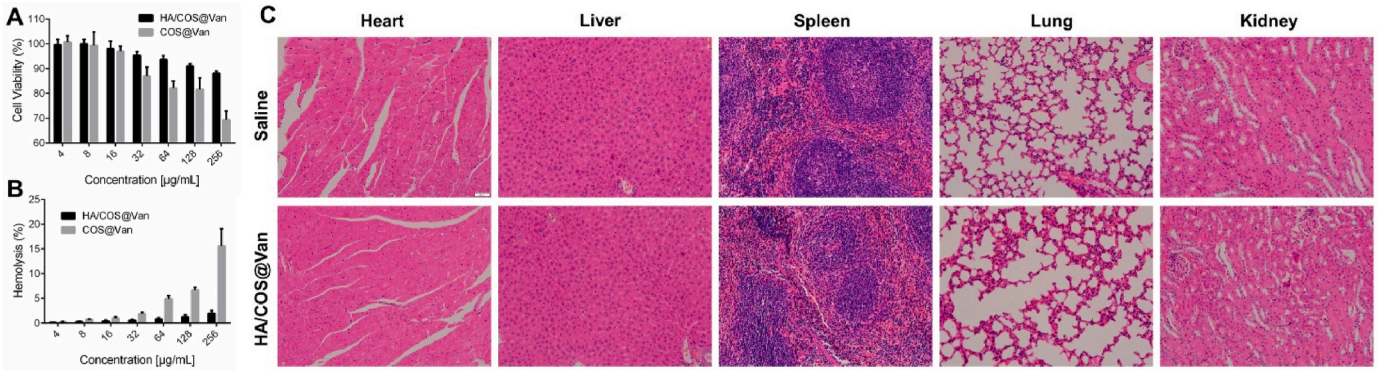

Fig. 5. Cell viability (A) and hemolysis analysis (B) following exposure to diverse concentrations of COS@Van and HA/COS@Van, respectively. The images of major organs after treatment with saline and HA/COS@Van in normal BALB/c mice (n = 6). Scale bars = 50 μm.

after a three-day treatment period with a dosage five times higher than the therapeutic level and were subsequently analyzed *via* H&E staining. Importantly, no mortality was observed in the treatment groups. Moreover, histological analysis of the major organs, including the liver, heart, spleen, kidneys, and lungs, revealed normal tissue morphology without any notable pathological changes (Fig. 5C). These results suggest that HA/COS@Van possesses favorable biocompatibility.

3.6. *In vivo* biodistribution and antibacterial effect in MRSA-infected mice

The tissue distribution of HA/COS *in vivo* was further investigated. BALB/c mice were intravenously injected with RHB-labeled HA/COS and COS NPs, and their distribution was monitored over time utilizing an IVIS imaging system. As depicted in Fig. 6A, in HA/COS NP-treated mice, strong RHB signals were detected in the liver during the 24-h treatment period, with subsequent accumulation observed in kidney, lung, and spleen. Notably, HA/COS exhibited rapid accumulation in the liver as early as 0.5 h post-injection, persisting for over 24 h. Although

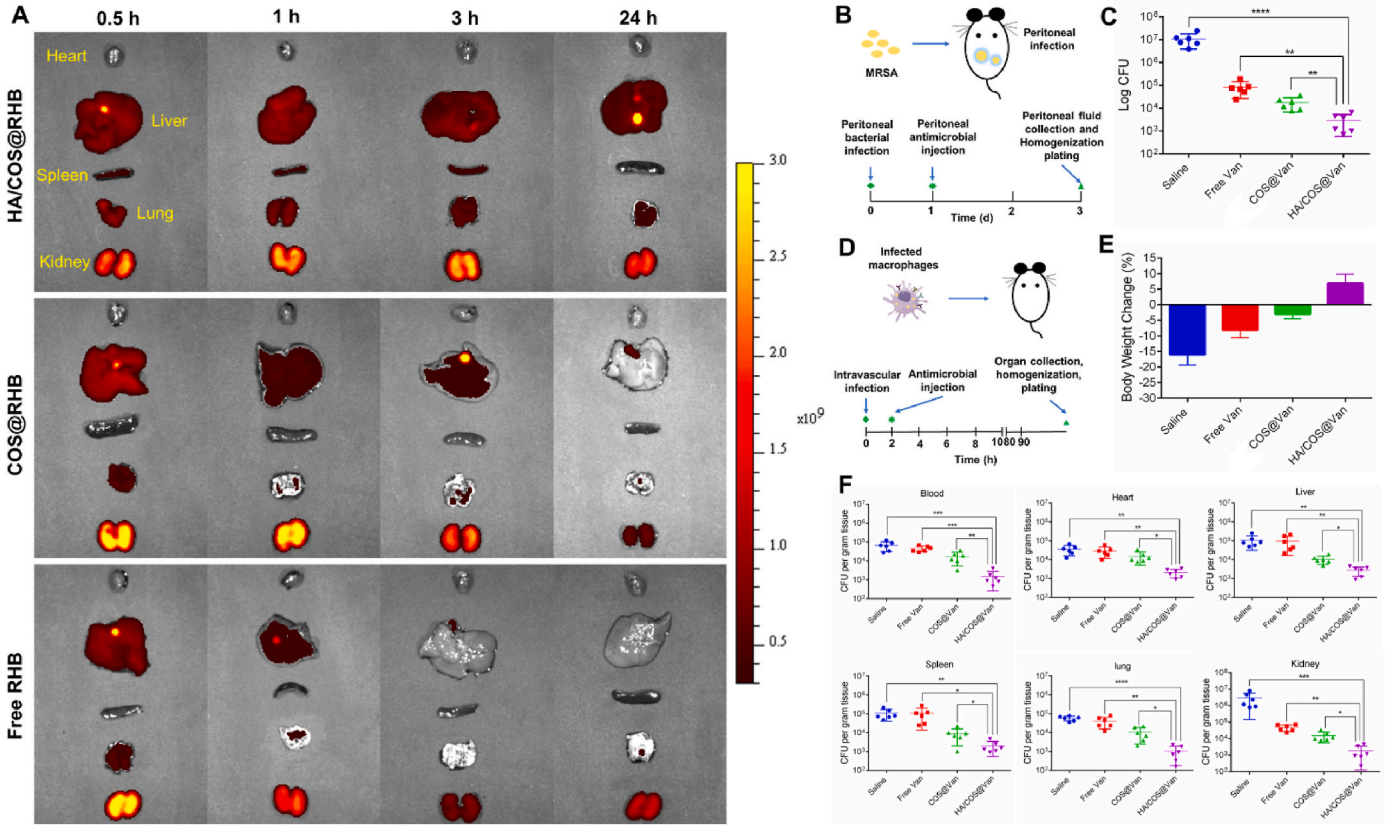

Fig. 6. *Ex vivo* visualization of primary organs 24 h post-administration (A). Diagram of the utilized mouse acute peritonitis model (B). Intracellular CFU count was obtained from peritoneal macrophages, which was extracted 48 h following intraperitoneal antimicrobial administration (C). Illustration of the employed mouse intravenous infection model. Organ infection was triggered by intravenous delivery of 200 μL suspension containing mouse macrophages with intracellular MRSA, succeeded 2 h later by intravenous administration of 200 μL saline or saline with Van, COS@Van, or HA/COS@Van (D). Mouse body weight over time post-treatment (E). CFU count retrieved from 1 g of homogenized organ tissue for various organs, excised 96 h after intravenous antimicrobial administration (F). Data are displayed as means ± standard deviations for 6 mice per group. Asterisks above data points denote statistical significance at $p < 0.05$ (*), $p < 0.01$ (**), $p < 0.001$ (***) and $p < 0.0001$ (****).

COS NPs also accumulated in the liver, the fluorescence intensity became undetectable after 24 h. It is well established that the liver serves as a primary organ where infected macrophages predominantly reside. Thus, HA/COS have the potential to preferentially deliver encapsulated antibiotics to macrophages, facilitating transport to bacterial infection sites *in vivo*.

The *in vivo* antibacterial efficacy of HA/COS@Van was initially evaluated using a peritonitis model induced by MRSA, a "serious threat" as classified by the U.S. CDC, and commonly employed as a representative model for intracellular infections [16,32]. To assess antibacterial effectiveness, the mice were euthanized 3 days post-infection (Fig. 6B). The highest intracellular CFU count was recorded from the plating of peritoneal macrophages following saline injection (Fig. 6C). Free Van treatment resulted in a 2 log-unit reduction in CFU counts relative to saline, whereas COS@Van further decreased the CFU count by an additional 1 log-unit. HA/COS@Van treatment demonstrated the greatest efficacy, reducing the peritoneal CFU count by 4 log-units compared to saline, markedly outperforming both COS@Van and free Van. Notably, HA/COS@Van exhibited a stronger inhibitory effect than COS@Van, which contrasts with the *in vitro* findings. The enhanced bactericidal activity observed *in vivo* for HA/COS@Van may be attributed to its targeted delivery mechanism. Although COS@Van has the potential to improve macrophage targeting *via* mannose-receptor interactions, the negatively charged tissue cells at the infection site may compete with macrophages for COS@Van, internalizing and sequestering them, thereby limiting their interaction with macrophages.

Macrophages harboring intracellular MRSA can disseminate through the bloodstream, leading to organ infections and exacerbating disease severity. Thus, the antimicrobial efficacy of HA/COS@Van was further assessed using a mouse model of organ infection, established by intravenous administration of infected macrophages with MRSA to facilitate systemic infection. Similarly, HA/COS@Van also proved more effective at eliminating organ infections in mice. As illustrated in Fig. 6D, 2 h after intravenous infection with MRSA-laden macrophages, mice were administered a single dose of saline, free Van, COS@Van, or HA/COS@Van. On day 4 post-treatment, the mice were sacrificed, and various organs were harvested, homogenized, and plated for analysis. No visible adverse effects were observed following HA/COS@Van administration, and the body weight of the mice remained stable throughout the experimental period until sacrifice (Fig. 6E), consistent with the lack of *in vitro* cytotoxicity previously noted (Fig. 5A). MRSA CFU counts per gram of homogenized organ tissue are presented in Fig. 6F for five organs and blood. HA/COS@Van achieved significant bacterial reduction, decreasing CFU counts by 1–3 log-units compared to saline across all organs. These results suggest that HA/COS@Van effectively inhibited the proliferation of intracellular MRSA *in vivo*.

4. Conclusions

In conclusion, HA/COS have been demonstrated to be an effective targeted delivery system, which is attributed to their HA coating. HA/COS specifically target MRSA-infected macrophages *in vitro*, and when utilized to eradicate intracellular MRSA, antibiotic-loaded HA/COS@-Van exhibits greater potency compared to free Van. In addition to its significant intracellular accumulation, HA/COS show the capacity to rapidly degrade within the acidic lysosomal environment, initiating an influx of water that disrupts lysosomal homeostasis. The released Van serves a crucial function in combating intracellular MRSA. When administered in a MRSA-induced peritonitis model and organ infection model, HA/COS@Van markedly enhances Van's efficacy. The remarkable effectiveness of HA/COS@Van suggests its potential for clinical success in treating intracellular MRSA infections.

CRediT authorship contribution statement

Wenting Li: Writing – original draft, Investigation, Data curation, Conceptualization. **WeiWei Li:** Investigation, Formal analysis. **Xuanxiang Zhai:** Methodology. **Xiao Liu:** Formal analysis. **Xiaoyi Shi:** Methodology. **Xiangjun Chen:** Supervision, Investigation, Funding acquisition. **Wei Hong:** Writing – review & editing, Supervision, Funding acquisition, Conceptualization.

Ethics approval and consent to participate

All procedures involving animals were conducted in compliance with the Guidelines for the Care and Use of Laboratory Animals at Binzhou Medical University and were approved by the Animal Ethics Committee of Binzhou Medical University.

Consent for publication

All authors agree to submit for publication in "Materials Today Bio".

Availability of data and materials

No datasets were generated or analyzed during the current study.

Funding

Financial support for this study was provided by the Taishan Scholar Foundation of Shandong Province (Grant No. tsqn201909143 and Grant No. tsqn202211230).

Declaration of competing interest

We declare that we have no financial and personal relationships with other people or organizations that can inappropriately influence our work, there is no professional or other personal interest of any nature or kind in any product, service and/or company that could be construed as influencing the position presented in, or the review of, the manuscript entitled "Bacteria Microenvironment-Responsive Vancomycin-Loaded Chitooligosaccharide Nanoparticles for Intracellular MRSA Infection Treatment"

Acknowledgements

Not applicable.

Appendix A. Supplementary data

Supplementary data to this article can be found online at https://doi.org/10.1016/j.mtbio.2025.101731.

Data availability

Data will be made available on request.

References

[1] S.Y. Tong, J.S. Davis, E. Eichenberger, T.L. Holland, V.G. Fowler Jr., Staphylococcus aureus infections: epidemiology, pathophysiology, clinical manifestations, and management, Clin. Microbiol. Rev. 28 (3) (2015) 603–661.
[2] B. Aslam, W. Wang, M.I. Arshad, M. Khurshid, S. Muzammil, M.H. Rasool, M. A. Nisar, R.F. Alvi, M.A. Aslam, M.U. Qamar, M.K.F. Salamat, Z. Baloch, Antibiotic resistance: a rundown of a global crisis, Infect. Drug Resist. 11 (2018) 1645–1658.
[3] F.R. DeLeo, M. Otto, B.N. Kreiswirth, H.F. Chambers, Community-associated meticillin-resistant Staphylococcus aureus, Lancet 375 (9725) (2010) 1557–1568.
[4] M. Kubica, K. Guzik, J. Koziel, M. Zarebski, W. Richter, B. Gajkowska, A. Golda, A. Maciag-Gudowska, K. Brix, L. Shaw, T. Foster, J. Potempa, A potential new pathway for Staphylococcus aureus dissemination: the silent survival of S. aureus phagocytosed by human monocyte-derived macrophages, PLoS One 3 (1) (2008) e1409.
[5] G.E. Thwaites, V. Gant, Are bloodstream leukocytes Trojan Horses for the metastasis of Staphylococcus aureus? Nat. Rev. Microbiol. 9 (3) (2011) 215–222.

[6] S. Carryn, H. Chanteux, C. Seral, M.P. Mingeot-Leclercq, F. Van Bambeke, P. M. Tulkens, Intracellular pharmacodynamics of antibiotics, Infect Dis Clin North Am 17 (3) (2003) 615–634.
[7] P.M. Tulkens, [Intracellular pharmacokinetics and pharmacodynamics of antibiotics], Rev. Pneumol. Clin. 52 (Suppl 2) (1996) S51–S55.
[8] P. Tulkens, A. Trouet, The uptake and intracellular accumulation of aminoglycoside antibiotics in lysosomes of cultured rat fibroblasts, Biochem. Pharmacol. 27 (4) (1978) 415–424.
[9] X. Kang, F. Bu, W. Feng, F. Liu, X. Yang, H. Li, Y. Yu, G. Li, H. Xiao, X. Wang, Dual-cascade responsive nanoparticles enhance pancreatic cancer therapy by eliminating tumor-resident intracellular bacteria, Adv. Mater. 34 (49) (2022) e2206765.
[10] Q. Li, Y. Chao, B. Liu, Z. Xiao, Z. Yang, Y. Wu, Z. Liu, Disulfiram loaded calcium phosphate nanoparticles for enhanced cancer immunotherapy, Biomaterials 291 (2022) 121880.
[11] H.J. Li, J.Z. Du, X.J. Du, C.F. Xu, C.Y. Sun, H.X. Wang, Z.T. Cao, X.Z. Yang, Y. H. Zhu, S. Nie, J. Wang, Stimuli-responsive clustered nanoparticles for improved tumor penetration and therapeutic efficacy, Proc. Natl. Acad. Sci. U. S. A. 113 (15) (2016) 4164–4169.
[12] L. Li, L. Zhang, T. Wang, X. Wu, H. Ren, C. Wang, Z. Su, Facile and scalable synthesis of novel spherical Au nanocluster Assemblies@Polyacrylic acid/calcium phosphate nanoparticles for dual-modal imaging-guided cancer chemotherapy, Small 11 (26) (2015) 3162–3173.
[13] F. Gao, L. Xu, B. Yang, F. Fan, L. Yang, Kill the real with the fake: eliminate intracellular Staphylococcus aureus using nanoparticle coated with its extracellular vesicle membrane as active-targeting drug carrier, ACS Infect. Dis. 5 (2) (2019) 218–227.
[14] X. Yang, B. Xie, H. Peng, G. Shi, B. Sreenivas, J. Guo, C. Wang, Y. He, Eradicating intracellular MRSA via targeted delivery of lysostaphin and vancomycin with mannose-modified exosomes, J. Contr. Release 329 (2021) 454–467.
[15] X. Yang, G. Shi, J. Guo, C. Wang, Y. He, Exosome-encapsulated antibiotic against intracellular infections of methicillin-resistant Staphylococcus aureus, Int. J. Nanomed. 13 (2018) 8095–8104.
[16] Y. Li, Y. Liu, Y. Ren, L. Su, A. Li, Y. An, V. Rotello, Z. Zhang, Y. Wang, Y. Liu, S. Liu, J. Liu, J.D. Laman, L. Shi, H.C. van der Mei, H.J. Busscher, Coating of a novel antimicrobial nanoparticle with a macrophage membrane for the selective entry into infected macrophages and killing of intracellular staphylococci, Adv. Funct. Mater. 30 (48) (2020).
[17] S. Rashki, K. Asgarpour, H. Tarrahimofrad, M. Hashemipour, M.S. Ebrahimi, H. Fathizadeh, A. Khorshidi, H. Khan, Z. Marzhoseyni, M. Salavati-Niasari, H. Mirzaei, Chitosan-based nanoparticles against bacterial infections, Carbohydr. Polym. 251 (2021) 117108.
[18] V.N. Davydova, I.M. Yermak, V.I. Gorbach, I.N. Krasikova, T.F. Solov'eva, Interaction of bacterial endotoxins with chitosan. Effect of endotoxin structure, chitosan molecular mass, and ionic strength of the solution on the formation of the complex, Biochemistry (Mosc) 65 (9) (2000) 1082–1090.
[19] F. Dong, S. Li, Wound dressings based on chitosan-dialdehyde cellulose nanocrystals-silver nanoparticles: mechanical strength, antibacterial activity and cytotoxicity, Polymers 10 (6) (2018).
[20] Y. Gutha, J.L. Pathak, W. Zhang, Y. Zhang, X. Jiao, Antibacterial and wound healing properties of chitosan/poly(vinyl alcohol)/zinc oxide beads (CS/PVA/ZnO), Int. J. Biol. Macromol. 103 (2017) 234–241.
[21] H. Iqbal, B.A. Khan, Z.U. Khan, A. Razzaq, N.U. Khan, B. Menaa, F. Menaa, Fabrication, physical characterizations and in vitro antibacterial activity of cefadroxil-loaded chitosan/poly(vinyl alcohol) nanofibers against Staphylococcus aureus clinical isolates, Int. J. Biol. Macromol. 144 (2020) 921–931.
[22] S.Y. Lee, M.S. Kang, W.Y. Jeong, D.W. Han, K.S. Kim, Hyaluronic acid-based theranostic nanomedicines for targeted cancer therapy, Cancers (Basel) 12 (4) (2020).
[23] Y. Yang, L. Jing, X. Li, L. Lin, X. Yue, Z. Dai, Hyaluronic acid conjugated magnetic prussian Blue@Quantum dot nanoparticles for cancer theranostics, Theranostics 7 (2) (2017) 466–481.
[24] H. Ji, K. Dong, Z. Yan, C. Ding, Z. Chen, J. Ren, X. Qu, Bacterial hyaluronidase self-triggered prodrug release for chemo-photothermal synergistic treatment of bacterial infection, Small 12 (45) (2016) 6200–6206.
[25] W. Li, Q. Fan, W. Cong, L. Wang, X. Li, W. Li, S. Hu, X. Chen, W. Hong, pH/hyal-responsive surface-charge switchable electrostatic complexation for efficient elimination of MRSA infection, Mol. Pharm. 20 (7) (2023) 3683–3692.
[26] X. Chen, X. Shi, X. Liu, X. Zhai, W. Li, W. Hong, Eliminating intracellular MRSA via mannosylated lipid-coated calcium phosphate nanoparticles, Mol. Pharm. 21 (11) (2024) 5772–5783.
[27] Y. Sun, J. Cui, L. Tian, Y. Mi, Z. Guo, Phenolic acid functional quaternized chitooligosaccharide derivatives: preparation, characterization, antioxidant, antibacterial, and antifungal activity, Mar. Drugs 21 (10) (2023).
[28] S.J. Wu, S.K. Pan, H.B. Wang, J.H. Wu, Preparation of chitooligosaccharides from cicada slough and their antibacterial activity, Int. J. Biol. Macromol. 62 (2013) 348–351.
[29] D. Ailincai, I. Rosca, S. Morariu, L. Mititelu-Tartau, L. Marin, Iminoboronate-chitooligosaccharides hydrogels with strong antimicrobial activity for biomedical applications, Carbohydr. Polym. 276 (2022) 118727.
[30] A.M. Piras, G. Maisetta, S. Sandreschi, M. Gazzarri, C. Bartoli, L. Grassi, S. Esin, F. Chiellini, G. Batoni, Chitosan nanoparticles loaded with the antimicrobial peptide temporin B exert a long-term antibacterial activity in vitro against clinical isolates of Staphylococcus epidermidis, Front. Microbiol. 6 (2015) 372.
[31] Z. Sobhani, S. Mohammadi Samani, H. Montaseri, E. Khezri, Nanoparticles of chitosan loaded ciprofloxacin: fabrication and antimicrobial activity, Adv. Pharmaceut. Bull. 7 (3) (2017) 427–432.
[32] S.L. Solomon, K.B. Oliver, Antibiotic resistance threats in the United States: stepping back from the brink, Am. Fam. Physician 89 (12) (2014) 938–941.